*17th World Conference on Earthquake Engineering, 17WCEE*
*Sendai, Japan - September 13th to 18th 2020*

# SEISMIC STABILITY ASSESSMENT OF STEEL MOMENT FRAMES AND IMPLICATIONS FOR DESIGN

L.A. Fahnestock[(1)], S. Shi[(2)], M.S. Speicher[(3)]

[(1)] *Professor, Civil and Environmental Engineering, University of Illinois at Urbana-Champaign, fhnstck@illinois.edu*
[(2)] *Graduate Research Assistant, Civil and Environmental Engineering, University of Illinois at Urbana-Champaign, shi40@illinois.edu*
[(3)] *Research Structural Engineer, Earthquake Engineering Group, National Institute of Standards and Technology, speicher@nist.gov*

## *Abstract*

Although it is clear that a building must be capable of carrying gravity loads while developing large inelastic deformations and associated lateral displacements during a large earthquake, achieving this performance objective in day-to-day practice still represents a major challenge. Current code-based consideration of seismic P-Delta effects is generally based on simplistic elastic models, and despite major advances in seismic systems and analysis techniques, no simple and reliable design methods for seismic stability are available.

Specific to steel buildings and the design framework in the United States, the current fundamental approach for stability design was developed and calibrated for non-seismic scenarios where the structure has modest overstrength and the ultimate strength (stability point) of the structure occurs prior to significant inelastic deformation. However, in a ductile steel seismic lateral force-resisting system (LFRS), the design-level forces and resulting nominally-elastic deformations are not consistent with the ultimate strength state of the system, which corresponds to significant overstrength and inelastic deformation.

Despite the vastly different behaviors expected in wind-dominated design vs. seismic-dominated design, the same stability design approach is employed. This stability design approach is nominally based on second-order elastic analysis (i.e., in the structural analysis model, equilibrium is formulated on the elastic deformed position and inelastic response is not considered). However, in seismic design it is not rational to consider P-Delta effects at elastic deformation levels.

The results described in this paper are part of a comprehensive study that is seeking to identify the most critical LFRS parameters that affect seismic stability and to develop a rigorous yet simple methodology whereby these parameters can be considered in design. This paper focuses on a set of steel special moment frames that is designed with or without consideration of stiffness reduction due to inelasticity, elastic P-Delta effects and drift limits. The moment frame designs are interrogated using nonlinear static and dynamic analyses to assess their collapse potential and to identify the most important parameters for design. The results from this paper will be combined with similar assessments for other types of steel seismic LFRS to propose design provisions that will enhance safety and economy for future design.

*Keywords: Steel Structures; Seismic Stability; Design Provisions*

## 1. Introduction

Seismic stability design has been studied for many years [1-3], and although modern performance-based seismic design does employ advanced analysis to rigorously consider stability effects, there has been relatively little advancement in how seismic stability is considered in pragmatic code-based procedures. In the United States, most buildings are designed for seismic loads using reduced forces based on the R factor prescribed in *Minimum Design Loads and Associated Criteria for Buildings and Other Structures* (ASCE/SEI 7-16) [4] with second-order elastic analysis – namely, the strength of the lateral force-resisting system (LFRS) is determined considering elastic P-Delta effects. However, research indicates that parameters related to inelastic response – such as post-yield stiffness and overstrength – are more important for seismic stability than initial elastic strength (i.e., the system yield strength).

Focusing on steel buildings and the *Specification for Structural Steel Buildings* (ANSI/AISC 360-16) [5], stability design is conducted with the direct analysis method (DM), which was developed and calibrated for non-seismic scenarios where the structure has modest overstrength and the ultimate strength (stability point) of the structure occurs prior to significant inelastic deformation. In a ductile steel seismic LFRS, such as a special moment frame (SMF), the design-level forces and resulting nominally-elastic deformations are not consistent with the ultimate strength state of the system, which corresponds to significant overstrength and inelastic deformation. Although the *Seismic Provisions for Structural Steel Buildings* (ANSI/AISC 341-16) [6] contain rigorous requirements related to capacity-based proportioning and ductile detailing, global seismic stability is not directly considered. The code-based seismic drift limit per ASCE 7 [4] is the primary means by which seismic stability is indirectly considered in the design process. In describing the seismic design landscape two decades ago, Gupta and Krawinkler [3] wrote, "At this time, no simple procedure can be recommended that will permit a definite assessment of collapse hazard due to P-Delta effects." Current code-based consideration of seismic stability has advanced little since that time, and a more fundamental approach is needed.

Several studies have provided preliminary insight into the effectiveness of current seismic design and assessment approaches. Buckling-restrained braced frame (BRBF) and BRBF-SMF dual systems were examined, and the study indicated that ignoring stiffness reduction, imperfections and (elastic) P-Delta effects in design while considering post-yield stiffness can provide acceptable seismic performance [7]. Furthermore, an earlier study examined SMFs and the effects of residual stresses and imperfections were shown to be unimportant for seismic response [8]. In a study that was focused on consistency between ASCE 7 and ASCE 41 [9] for BRBF, SMF, special concentrically-braced frame (SCBF) and eccentrically-braced frame (EBF) systems, nonlinear models were used to assess the performance of code-compliant buildings [10-14]. In general, the results indicate that the ASCE 41 assessment procedure is overly conservative and that collapse performance evaluated with the *Quantification of Building Seismic Performance Factors* FEMA P695 methodology [15] is generally acceptable for buildings designed per ASCE 7.

This paper summarizes the initial portion of a study that is comprehensively evaluating seismic stability design of steel frames. A series of code-compliant and non-code-compliant SMFs were designed and evaluated with nonlinear static (pushover) and nonlinear dynamic (response history) analyses. Differences in observed response are discussed and implications for future work are presented.

## 2. Building Designs and Numerical Models

### 2.1 Prototype Building Designs

The 8-story and 16-story office buildings referenced in NIST Technical Note 1863-1 [16] were the basis of the prototype buildings designed for this research. As shown in Fig. 1 for the 8-story building, the rectangular plan of the prototype buildings contains two perimeter 3-bay SMFs in the East-West direction and four perimeter SCBFs in the North-South direction. The research reported here focuses on the SMFs only, and the designs are based on ASCE 7-16, which leads to small variations compared to the original

NIST designs that were based on ASCE 7-05. All other parameters for the prototype building are consistent with NIST Technical Note 1863-1 [16]. Along with ASCE 7-16, AISC 341-16 and AISC 360-16 were used to design the prototype buildings. Stability was considered in accordance with the Direct Analysis Method (DM) in Ch. C of AISC 360-16 [5], which includes elastic P-Delta effects and stiffness reduction. There are two basic approaches for seismic lateral force analysis in ASCE 7-16: the equivalent lateral force procedure (ELF) and modal response spectrum analysis (RSA). ELF approximates a first-mode force profile, whereas RSA includes contributions from multiple modes. In both approaches, the analyses are elastic (no material nonlinearity) but do included geometric nonlinearity (P-Delta effects).

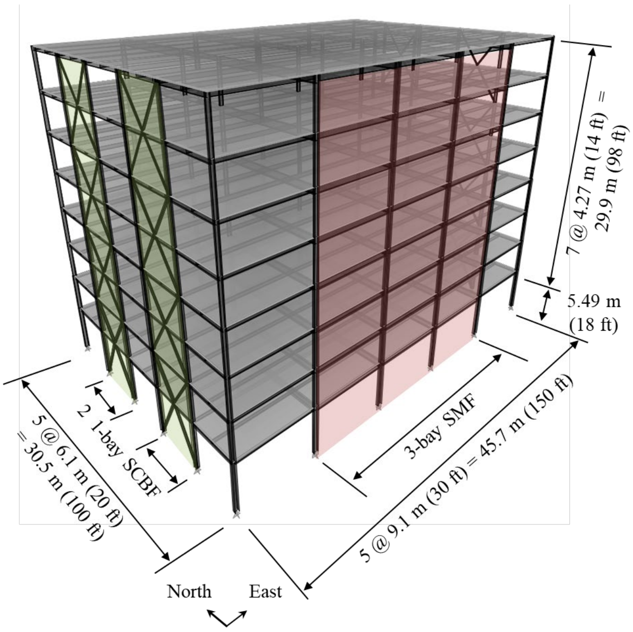


Fig. 1 – 8-story Prototype Building

The frame design matrix is based on code-compliant designs that use second-order elastic analysis. From this baseline design, variations are made to study the effect of analysis type (first-order elastic) and the effect of a seismic drift limit. Table 1 shows the design matrix, where FO represents a non-code-compliant design ignoring stiffness reduction and P-Delta effects, and SO represents a code-compliant design. An asterisk indicates a design that ignores the drift limit. Table 1 indicates that the controlling requirement of all 16-story SMFs was strength (and drift was satisfied automatically). A summary of frame member sections is provided in Tables 2 and 3, and seismic design parameters are presented in Table 4. The dead load calculation considered self-weight for each design, so seismic weights (D + 0.2L) are slightly different within each building scenario. $V_{design}$ is the base shear for strength design and $V_{drift}$ is the base shear for the drift check. For reference, the story drift profiles under drift check lateral forces are shown in Fig. 2.

Table 1 – Design Matrix of Special Moment Frames

| **Analysis Type** | **Drift Check** | **8-Story** | | **16-Story** | |
|---|---|---|---|---|---|
| | | **ELF** | **RSA** | **ELF** | **RSA** |
| First-Order | Yes | 08-ELF-FO | 08-RSA-FO | 16-ELF-FO | 16-RSA-FO |
| Second-Order | Yes | 08-ELF-SO | 08-RSA-SO | 16-ELF-SO | 16-RSA-SO |
| First-Order | No | 08-ELF-FO* | 08-RSA-FO* | – | – |
| Second-Order | No | 08-ELF-SO* | 08-RSA-SO* | – | – |

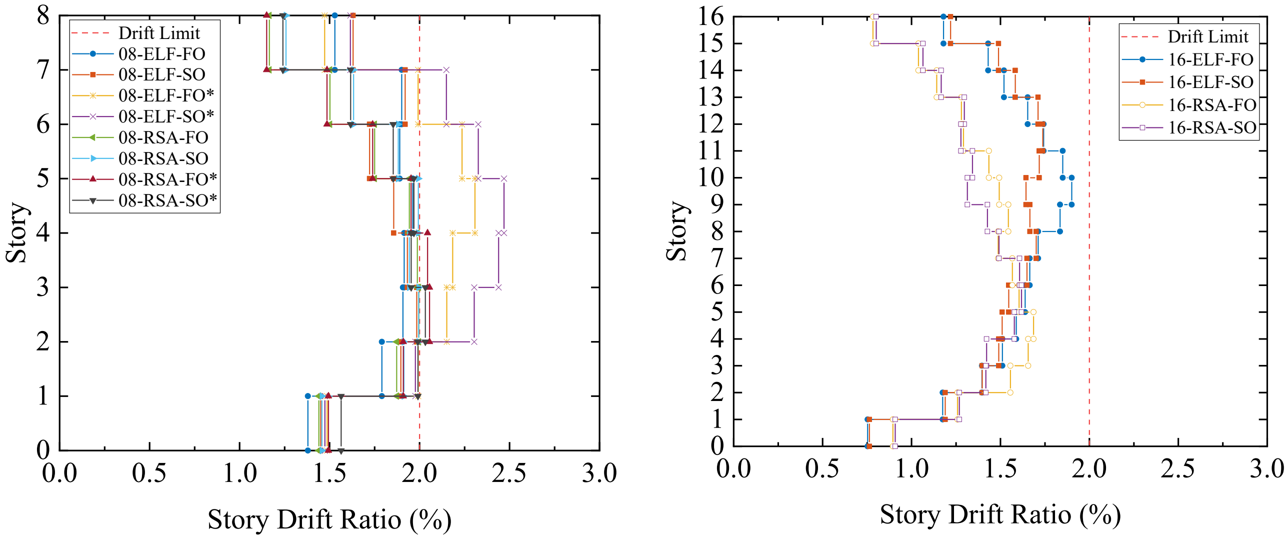


(a) (b)

Fig. 2 – Design Story Drift Ratio Profiles: (a) 8-story SMFs; (b) 16-story SMFs

Table 2 – 8-Story Special Moment Frame Designs

| Level | Beam | Interior Column | Exterior Column | Beam | Interior Column | Exterior Column |
|---|---|---|---|---|---|---|
| | | 8-ELF-FO | | | 8-ELF-SO | |
| 8th /Roof | W 24 × 55 | W 18 × 143 | W 18 × 86 | W 24 × 55 | W 18 × 143 | W 18 × 86 |
| 6th /7th | W 27 × 94 | W 18 × 234 | W 18 × 119 | W 30 × 108 | W 18 × 258 | W 18 × 143 |
| 4th /5th | W 30 × 108 | W 18 × 258 | W 18 × 143 | W 30 × 116 | W 18 × 283 | W 18 × 175 |
| 2nd / 3rd | W 30 × 108 | W 18 × 258 | W 18 × 192 | W 30 × 116 | W 18 × 283 | W 18 × 211 |
| | | 8-ELF-FO* | | | 8-ELF-SO* | |
| 8th /Roof | W 24 × 55 | W 18 × 143 | W 18 × 86 | W 24 × 55 | W 18 × 143 | W 18 × 86 |
| 6th /7th | W 24 × 76 | W 18 × 192 | W 18 × 106 | W 24 × 84 | W 18 × 211 | W 18 × 143 |
| 4th /5th | W 27 × 94 | W 18 × 234 | W 18 × 143 | W 27 × 94 | W 18 × 234 | W 18 × 158 |
| 2nd /3rd | W 27 × 94 | W 18 × 234 | W 18 × 192 | W 30 × 108 | W 18 × 258 | W 18 × 192 |
| | | 8-RSA-FO | | | 8-RSA-SO | |
| 8th /Roof | W 24 × 55 | W 18 × 143 | W 18 × 86 | W 24 × 55 | W 18 × 143 | W 18 × 86 |
| 6th /7th | W 24 × 76 | W 18 × 192 | W 18 × 106 | W 24 × 84 | W 18 × 211 | W 18 × 143 |
| 4th /5th | W 27 × 94 | W 18 × 234 | W 18 × 143 | W 27 × 94 | W 18 × 234 | W 18 × 158 |
| 2nd / 3rd | W 27 × 94 | W 18 × 234 | W 18 × 192 | W 30 × 108 | W 18 × 258 | W 18 × 192 |
| | | 8-RSA-FO* | | | 8-RSA-SO* | |
| 8th /Roof | W 21 × 44 | W 18 × 119 | W 18 × 55 | W 21 × 44 | W 18 × 119 | W 18 × 55 |
| 6th /7th | W 24 × 55 | W 18 × 143 | W 18 × 65 | W 24 × 55 | W 18 × 143 | W 18 × 86 |
| 4th /5th | W 24 × 62 | W 18 × 175 | W 18 × 97 | W 24 × 76 | W 18 × 192 | W 18 × 106 |
| 2nd / 3rd | W 24 × 76 | W 18 × 192 | W 18 × 130 | W 24 × 84 | W 18 × 211 | W 18 × 158 |



 

Table 3 – 16-Story Special Moment Frame Designs

| Level | Beam | Interior Column | Exterior Column | Beam | Interior Column | Exterior Column |
|---|---|---|---|---|---|---|
| | 16-ELF-FO (16-ELF-FO*) | | | 16-ELF-SO (16-ELF-SO*) | | |
| 16th /Roof | W 24 × 55 | W 27 × 129 | W 27 × 94 | W 24 × 55 | W 27 × 129 | W 27 × 94 |
| 14th /15th | W 27 × 94 | W 27 × 235 | W 27 × 114 | W 27 × 94 | W 27 × 235 | W 27 × 114 |
| 12th /13th | W 30× 108 | W 27 × 258 | W 27 × 129 | W 30× 108 | W 27 × 258 | W 27 × 194 |
| 10th /11th | W 30× 108 | W 27 × 258 | W 27 × 194 | W 33× 130 | W 27 × 307 | W 27 × 235 |
| 8th /9th | W 33× 130 | W 27 × 307 | W 27 × 194 | W 33× 130 | W 27 × 307 | W 27 × 235 |
| 6th /7th | W 33× 130 | W 27 × 307 | W 27 × 258 | W 33× 152 | W 27 × 368 | W 27 × 336 |
| 4th /5th | W 33× 130 | W 27 × 368 | W 27 × 307 | W 33× 152 | W 27 × 368 | W 27 × 336 |
| 2nd / 3rd | W 33× 130 | W 27 × 368 | W 27 × 539 | W 33× 152 | W 27 × 368 | W 27 × 539 |
| | 16-RSA-FO (16-RSA-FO*) | | | 16-RSA-SO (16-RSA-SO*) | | |
| 16th /Roof | W 24 × 55 | W 27 × 129 | W 27 × 94 | W 24 × 55 | W 27 × 129 | W 27 × 94 |
| 14th /15th | W 24 × 76 | W 27 × 178 | W 27 × 94 | W 24 × 76 | W 27 × 235 | W 27 × 102 |
| 12th /13th | W 27 × 94 | W 27 × 235 | W 27 × 102 | W 27 × 94 | W 27 × 235 | W 27 × 102 |
| 10th /11th | W 27 × 94 | W 27 × 235 | W 27 × 102 | W 30× 108 | W 27 × 258 | W 27 × 129 |
| 8th /9th | W 30× 108 | W 27 × 258 | W 27 × 129 | W 30× 108 | W 27 × 258 | W 27 × 129 |
| 6th /7th | W 30× 108 | W 27 × 258 | W 27 × 129 | W 30× 108 | W 27 × 258 | W 27 × 146 |
| 4th /5th | W 30× 108 | W 27 × 258 | W 27 × 146 | W 33× 130 | W 27 × 307 | W 27 × 161 |
| 2nd / 3rd | W 33× 130 | W 27 × 307 | W 27 × 217 | W 33× 130 | W 27 × 307 | W 27 × 235 |

Table 4 – Summary of Seismic Design Parameters for Prototype Building in East-West direction

| Case | $W_{total}$ (kips) | $W_{SMF}$ (kips) | $V_{design}$ (kips) | $V_{drift}$ (kips) | $C_uT_a$ (s) | $T_1$ (s) |
|---|---|---|---|---|---|---|
| 08-ELF-FO | 10651 | 299 | 513 | 333 | 1.76 | 2.60 |
| 08-ELF-SO | 10679 | 327 | 514 | 338 | 1.76 | 2.42 |
| 08-ELF-FO* | 10623 | 271 | 512 | – | 1.76 | 2.97 |
| 08-ELF-SO* | 10642 | 290 | 513 | – | 1.76 | 2.77 |
| 08-RSA-FO | 10566 | 211 | 509 | 240 | 1.76 | 3.80 |
| 08-RSA-SO | 10581 | 219 | 509 | 230 | 1.76 | 3.53 |
| 08-RSA-FO* | 10555 | 201 | 509 | – | 1.76 | 3.82 |
| 08-RSA-SO* | 10573 | 218 | 509 | – | 1.76 | 3.58 |
| 16-ELF-FO | 21828 | 788 | 958 | 442 | 3.02 | 3.90 |
| 16-ELF-SO | 21897 | 860 | 961 | 447 | 3.02 | 3.63 |
| 16-RSA-FO | 21652 | 608 | 951 | 372 | 3.02 | 4.82 |
| 16-RSA-SO | 21679 | 638 | 953 | 358 | 3.02 | 4.54 |

## 2.2 Numerical Models

The OpenSees framework [17] was used to carry out the nonlinear static (pushover) analyses and nonlinear dynamic (response history) analyses of the SMF models. Given that the lateral force-resisting frames are located at the perimeter and the building is symmetric, the numerical models were 2D. Modal damping of 3% was used and an additional 0.3% stiffness-proportional damping was applied to damp out higher modes. Nonlinear rotational springs were placed at the ends of the SMF columns (half the column depth from the face of the beam) and at the center of each reduced beam section (RBS) connection. The nonlinear springs use the modified Ibarra Medina Krawinkler (IMK) deterioration model, which simulates in-cycle and cyclic degradation [18]. The force-deformation parameters for the RBS connections followed the recommendations made by Lignos and Krawinkler [19], which were derived using multivariate regression analysis of a database of experimental results. The force-deformation parameters for the column hinges followed the recommendations produced by NIST [20] using a monotonic backbone. The panel zones were modeled using the approach outlined by Krawinkler [21]. Additionally, although the column splice was designed at 1.2 m (4 ft) above the beam-to-column joint, this was ignored in the model and section size changes were made at the floor levels.

To approximately capture the behavior of the gravity framing system, a leaning column was used. The leaning column was assigned a moment of inertia equal to the sum of the moments of inertia of the tributary gravity frame columns and SCBF columns. The leaning column was attached to each floor of the SMF using equal degree of freedom constraints in the horizontal direction. Additionally, elastic-plastic hinges were placed at the top and bottom of each story and assigned a strength equal to the sum of the plastic moments of the non-SMF columns.

## 3. Numerical Simulations

### 3.1 Nonlinear Static Analyses

Nonlinear static analyses were performed to evaluate and compare behavior of the prototype designs. Based on the nonlinear analysis procedures described in FEMA P695 [15], the gravity loading applied in the numerical models was 1.05D + 0.25L, and the lateral load distribution was in proportion to the fundamental mode shape. Pushover curves (base shear vs. roof drift ratio) are shown in Fig. 3, with the following three important points marked: a) end of the linear range, b) peak base shear ($V_{max}$), and c) $0.8V_{max}$. These curves demonstrate that all frames exhibit significant softening around 1% roof drift ratio and reach $V_{max}$ between 1% and 2% roof drift ratio. Beyond $V_{max}$, significant negative stiffness develops due to the global P-Delta effects. Response quantities from the pushover analyses provide useful comparisons between the prototype designs. Ultimate displacement ($\delta_u$) is defined as the roof displacement at $0.8V_{max}$, and the effective yield displacement ($\delta_{y,eff}$) is calculated per FEMA P695 [15] and used as a reference for defining ductility as $\mu = \delta_u / \delta_{y,eff}$. System overstrength is defined as $\Omega = V_{max} / V_{design}$. A summary of these response quantities is provided in Table 5.

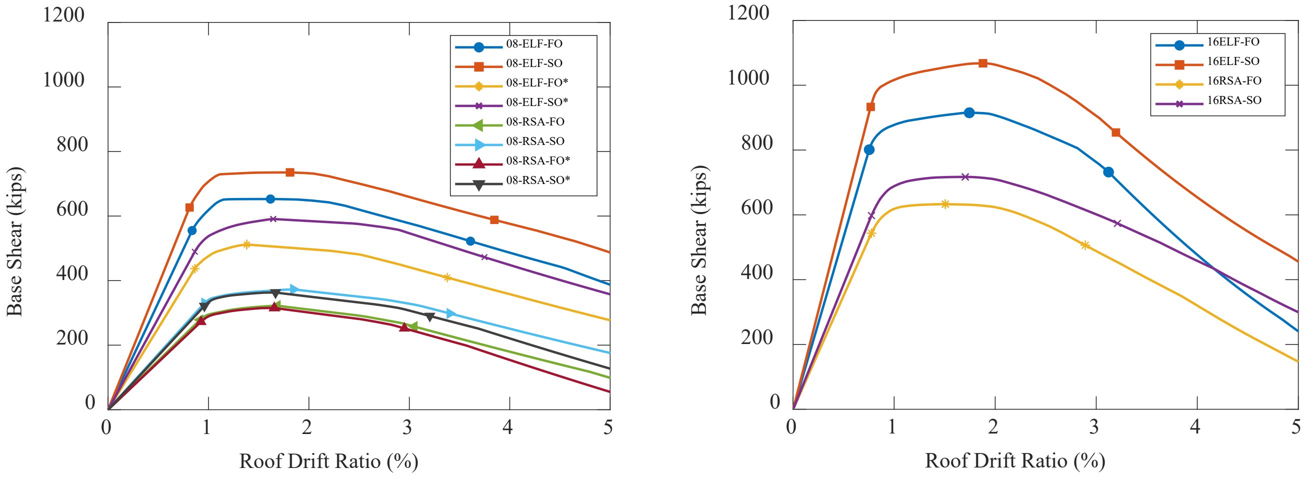


(a) 8-story SMFs (b) 16-story SMFs

Fig. 3 – Pushover Curves



 

Table 5 – Summary of Response Quantities of One Perimeter Frame from Pushover Analyses

| Case | $V_{design}$ (kips) | $V_{drift}$ (kips) | $V_{max}$ (kips) | $\delta_{y,eff}$ / h (%) | $\delta_u$ / h (%) | Ω | μ | $K_1$ (k/in) |
|---|---|---|---|---|---|---|---|---|
| 08-ELF-FO | 256 | 167 | 653 | 0.98 | 3.61 | 2.54 | 3.67 | 47.6 |
| 08-ELF-SO | 257 | 169 | 735 | 0.95 | 3.85 | 2.86 | 4.04 | 55.4 |
| 08-ELF-FO* | 256 | – | 512 | 1.01 | 3.38 | 2.00 | 3.34 | 36.3 |
| 08-ELF-SO* | 256 | – | 591 | 1.04 | 3.75 | 2.31 | 3.60 | 40.7 |
| 08-RSA-FO | 254 | 120 | 322 | 1.06 | 3.05 | 1.27 | 2.88 | 21.8 |
| 08-RSA-SO | 255 | 115 | 373 | 1.08 | 3.40 | 1.46 | 3.14 | 24.7 |
| 08-RSA-FO* | 254 | – | 315 | 1.07 | 2.95 | 1.24 | 2.76 | 21.1 |
| 08-RSA-SO* | 254 | – | 363 | 1.08 | 3.20 | 1.43 | 2.96 | 24.1 |
| 16-ELF-FO | 479 | 221 | 915 | 0.86 | 3.12 | 1.91 | 3.63 | 38.9 |
| 16-ELF-SO | 481 | 224 | 1068 | 0.88 | 3.20 | 2.22 | 3.64 | 44.4 |
| 16-RSA-FO | 476 | 186 | 633 | 0.90 | 2.89 | 1.33 | 3.21 | 25.6 |
| 16-RSA-SO | 476 | 179 | 717 | 0.93 | 3.21 | 1.50 | 3.46 | 28.2 |

As shown in Table 5, $V_{design}$ is essentially equal for designs of the same building using ELF and RSA, but Ω is significantly reduced for RSA designs compared to ELF designs. For the two code-compliant ELF designs, Ω is greater than 2, whereas for the two code-compliant RSA designs, Ω is around 1.5. For the code-compliant designs, the 8-story ELF design has approximately 30% greater μ than the RSA design, whereas the 16-story ELF design has only 5% greater μ than the RSA design. The impact of these differences in overstrength and ductility, in conjunction with other parameters, requires further investigation through dynamic analysis.

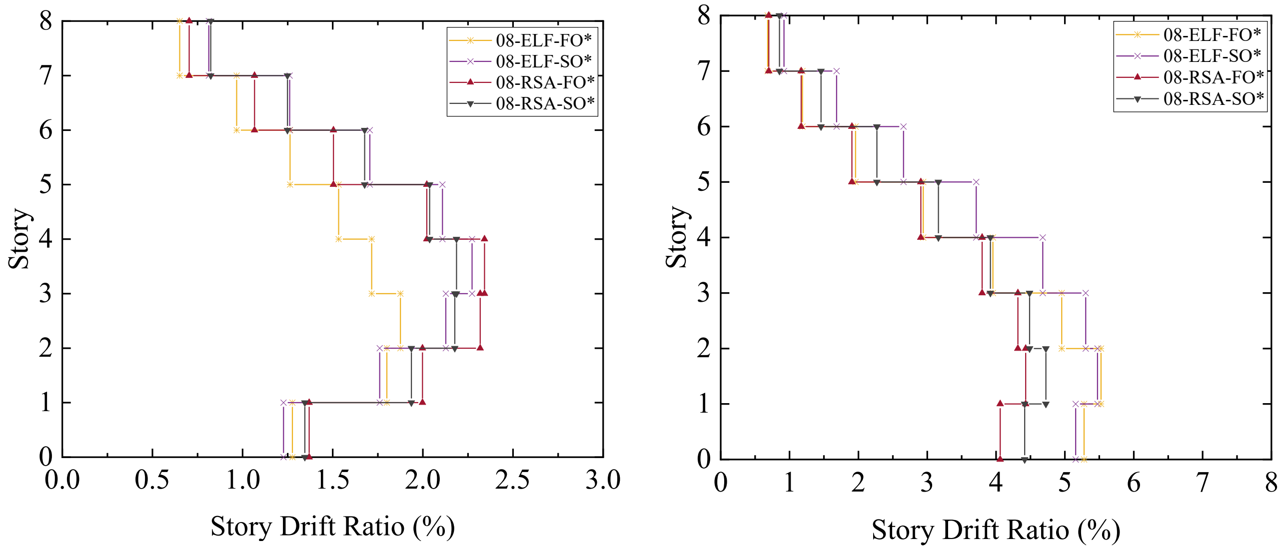


(a) At Maximum Base Shear Capacity ($V_{max}$) (b) At Ultimate Displacement ($\delta_u$)

Fig. 4 – Effect of Analysis Type on Story Drift Profile of 8-story SMFs without Drift Limit

The influences of analysis type on the distributions of inelasticity in the pushover analyses are presented in the story drift profiles taken at the points of $V_{max}$ and $\delta_u$, as shown in Fig. 4, Fig. 5 and Fig. 6. These figures demonstrate that story drift was generally concentrated in the middle stories at the points of maximum base shear, and then drift became more pronounced in the lower stories in the region of global negative stiffness. The shape of the story drift profiles of SMFs designed considering elastic P-Delta effects are similar to the cases designed without elastic P-Delta effects. Comparison of the 8-story ELF designs with and without drift limits indicates that stiffening of the frame in the middle stories to meet drift limits leads to greater concentration of inelastic demands in the lower stories. However, this is not observed in the 8-story RSA designs, which consider higher modes of response.

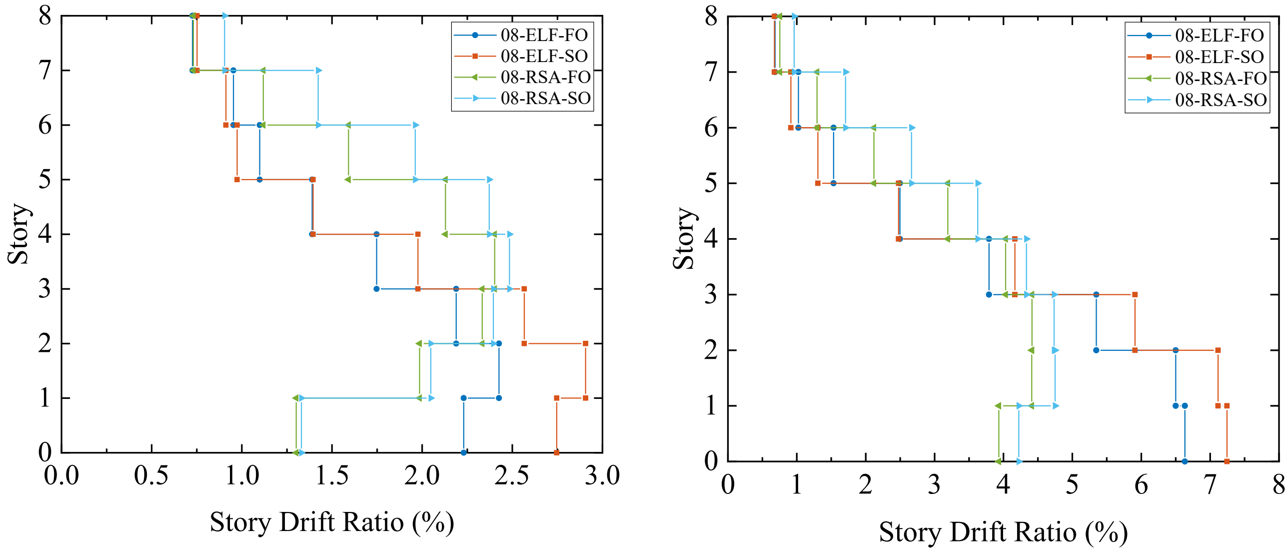


(a) At Maximum Base Shear Capacity ($V_{max}$) (b) At Ultimate Displacement ($\delta_u$)

Fig. 5 – Effect of Analysis Type on Story Drift Profile of 8-story SMFs from Pushover Analyses

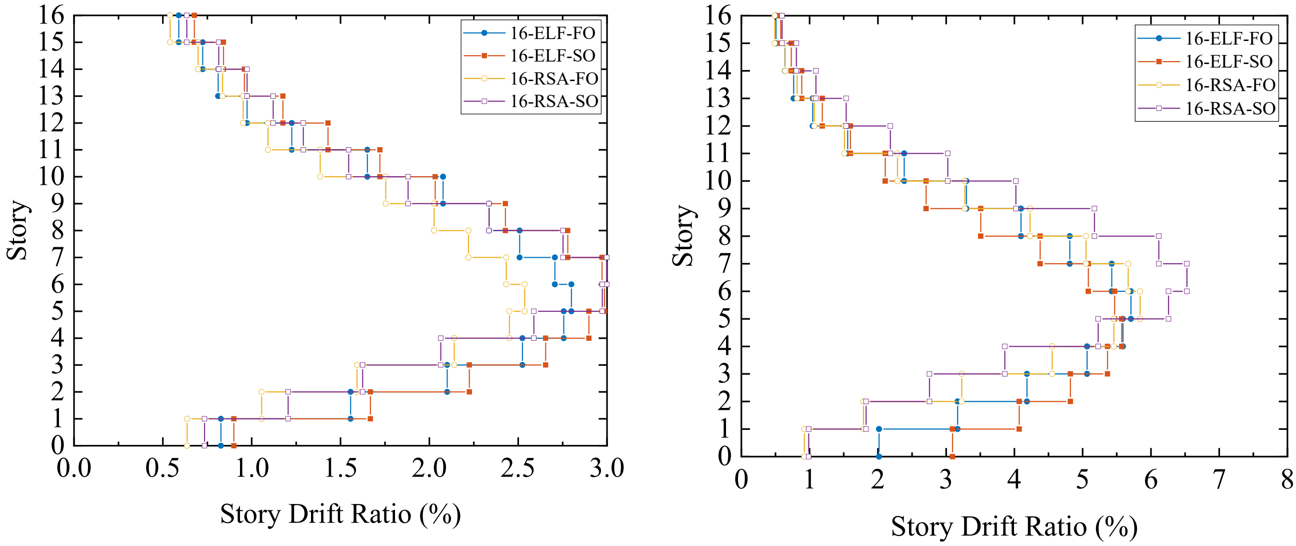


(a) At Maximum Base Shear Capacity ($V_{max}$) (b) At Ultimate Displacement ($\delta_u$)

Fig. 6 – Effect of Analysis Type on Story Drift Profile of 16-story SMFs from Pushover Analyses

The effects of drift limit and analysis type on response quantities are summarized in Table 6 and Table 7, respectively, by calculating the ratios of response quantities. Comparing cases with and without drift limit for the 8-story designs, removing the drift limit is seen to reduce the weight of steel in the special moment frame ($W_{SMF}$) by 11% in the code-compliant ELF design, but only 1% in the code-compliant RSA design. Correspondingly, $V_{max}$ was reduced by 20% in the ELF design and only 3% in the RSA design. The drift limit has a significant impact on initial stiffness for the ELF design (over 30%), but minimal impact for the RSA design (less than 5%).



 

Considering the impact of P-Delta effects (second-order analysis), which also includes stiffness reduction per the Direct Analysis Method (DM), Table 7 shows an increase of $W_{SMF}$ roughly in the range of 5-10%. This increased steel weight translates into increases in strength of roughly 10-15% and increases in ductility of roughly 5-10%. The pushover curves in Fig. 3 illustrate these increases graphically, and the increases in elastic stiffness are also evident. Elastic stiffness increases are approximately on the same order as the strength increases (10-15%).

Table 6 – Effect of Drift Limit on Response Quantities from Pushover Analyses

| **Case** | $\frac{(W_{SMF})^*}{(W_{SMF})}$ | $\frac{(V_{max})^*}{(V_{max})}$ | $\frac{(\Omega)^*}{(\Omega)}$ | $\frac{(\mu)^*}{(\mu)}$ | $\frac{(K_1)^*}{(K_1)}$ |
|---|---|---|---|---|---|
| 08-ELF-FO*/08-ELF-FO | 0.91 | 0.78 | 0.79 | 0.91 | 0.76 |
| 08-ELF-SO*/08-ELF-SO | 0.89 | 0.80 | 0.81 | 0.89 | 0.73 |
| 08-RSA-FO*/08-RSA-FO | 0.95 | 0.98 | 0.98 | 0.96 | 0.97 |
| 08-RSA-SO*/08-RSA-SO | 0.99 | 0.97 | 0.97 | 0.94 | 0.97 |

Table 7 – Effect of Analysis Type on Response Quantities from Pushover Analyses

| **Case** | $\frac{(W_{SMF})_{FO}}{(W_{SMF})_{SO}}$ | $\frac{(V_{max})_{FO}}{(V_{max})_{SO}}$ | $\frac{(\Omega)_{FO}}{(\Omega)_{SO}}$ | $\frac{(\mu)_{FO}}{(\mu)_{SO}}$ | $\frac{(K_1)_{FO}}{(K_1)_{SO}}$ |
|---|---|---|---|---|---|
| 08-ELF-FO/08-ELF-SO | 0.91 | 0.89 | 0.89 | 0.91 | 0.86 |
| 08-ELF-FO*/08-ELF-SO* | 0.93 | 0.87 | 0.87 | 0.93 | 0.89 |
| 08-RSA-FO/08-RSA-SO | 0.96 | 0.86 | 0.86 | 0.92 | 0.88 |
| 08-RSA-FO*/08-RSA-SO* | 0.92 | 0.87 | 0.87 | 0.93 | 0.88 |
| 16-ELF-FO/16-ELF-SO | 0.92 | 0.86 | 0.86 | 1.00 | 0.88 |
| 16-RSA-FO/16-RSA-SO | 0.95 | 0.88 | 0.88 | 0.93 | 0.91 |

### 3.2 Nonlinear Response History Analyses

To further evaluate the influence of LFRS design parameters on seismic performance, the 8-story ELF designs were subjected to the far-field record set (44 individual horizontal ground motions) from FEMA P695. The ground motions were normalized per FEMA P695 then the median spectral ordinate of these 44 ground motions scaled to match the acceleration of the risk-targeted MCE response spectrum at the target fundamental period for the building ($C_uT_a$, tabulated in Table 4).

Table 8 – Median Response Quantities under MCE Ground Motions

| **Case** | **Peak Story Shear (kips)** | **Peak Roof Drift Ratio (%)** | **Peak Story Drift Ratio (%)** |
|---|---|---|---|
| 08-ELF-FO | 873 | 1.87 | 3.14 |
| 08-ELF-SO | 945 | 1.77 | 3.21 |
| 08-ELF-FO* | 763 | 2.00 | 3.35 |
| 08-ELF-SO* | 859 | 1.93 | 3.42 |

Median response quantities for the set of nonlinear dynamic analyses are summarized in Table 8. For the code-compliant design (08-ELF-SO), the median peak roof drift ratio is 1.77% and the median peak story drift ratio is 3.21%. Considering that the design basis earthquake (DBE) is approximately 2/3 of the MCE, the MCE response indicates a median DBE response around the design target of 2%. Comparing 08-ELF-FO to 08-ELF-SO, the design including P-Delta is seen to have a slightly smaller median peak roof drift ratio, but a slightly larger median peak story drift ratio. This somewhat unusual result arises due to the larger section sizes that are used in the SO design, which lead to redistribution of inelastic response.

The designs without drift limit clearly experience greater inelastic drifts than their counterpart designs with drift limits. In the scenario considered here, the drift limit appears to be more influential than consideration of P-Delta effects. The design by first-order analysis that considers the drift limit (08-ELF-FO) performs better than the design by second-order analysis that ignores the drift limit (08-ELF-SO*). Fig. 7 shows that 08-ELF-FO has the most uniform distribution of drift of the four cases considered. Referring back to Fig. 4 and Fig. 5, the story drift profiles from pushover analyses, which use an elastic first mode force profile, have greater variation. The drift limit, which led to larger section sizes in the middle stories, reduced story drift ratios in this region, but also increased story drift ratios above and below.

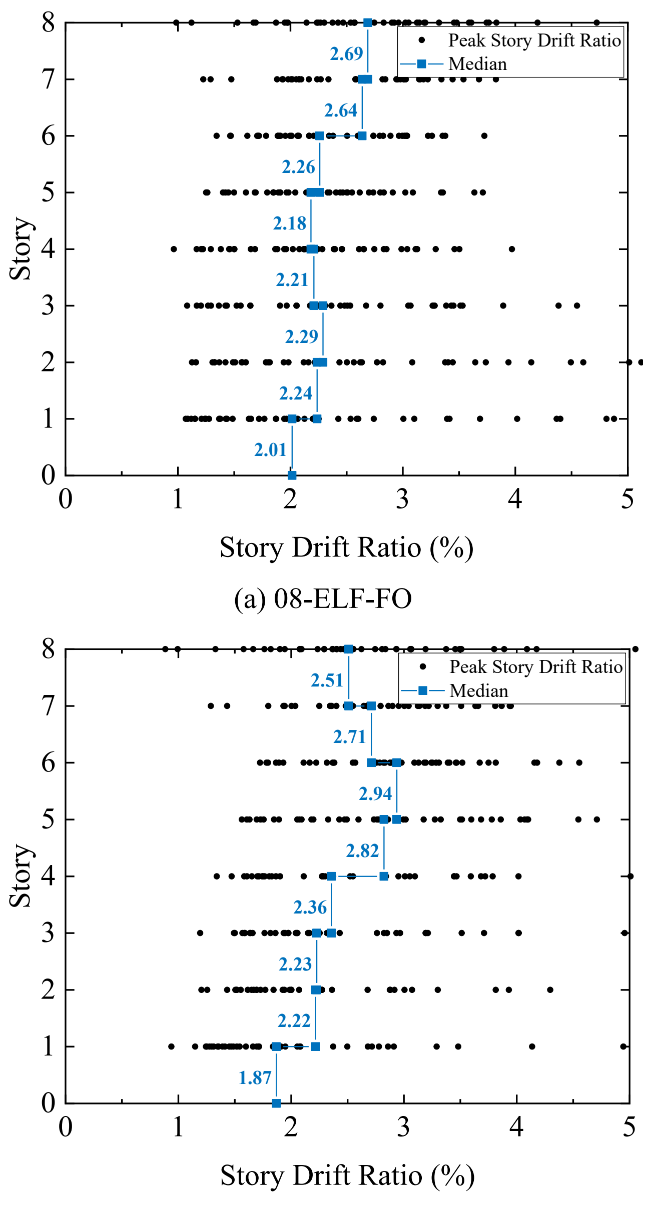


(a) 08-ELF-FO (b) 08-ELF-SO

(c) 08-ELF-FO* (d) 08-ELF-SO*

Fig. 7 – Median Peak Story Drift Profile under MCE Ground Motion



 

## 4. Summary

The ongoing research project described in this paper aims to identify the most critical LFRS parameters that affect seismic stability and to develop a rigorous yet simple methodology whereby these parameters can be considered in design. This paper focuses on a set of steel special moment frames (SMF) that is designed with or without consideration of stiffness reduction due to inelasticity, elastic P-Delta effects and drift limits. Office buildings with two heights (8-story and 16-story) were based on prior work conducted at NIST and designed using current code provisions in the United States. The buildings have regular plan configurations with perimeter lateral force-resisting frames. Equivalent lateral force (ELF) and modal response spectrum analysis (RSA) procedures were used in the design process. The moment frame designs are interrogated using nonlinear static and dynamic analyses to assess their collapse potential and to identify the most important parameters for design. Several observations from the present study are:

- For the 8-story case, removing the drift limit reduces the weight of steel in the SMF by 11% in the code-compliant ELF design, but only 1% in the code-compliant RSA design. From pushover analyses, the peak base shear was reduced by 20% in the ELF design and 3% in the RSA design.
- For the 8-story cases, the drift limit has a significant impact on initial stiffness for the ELF design (over 30%), but minimal impact for the RSA design (less than 5%). For the 16-story cases, the drift limit was not influential since it was satisfied based only on strength requirements.
- Enforcing the drift limit for the 8-story cases led to larger member sizes in the middle stories. This increase in stiffness and strength reduced inelastic dynamic response in stories 4-7, but increased the response above and below.
- Considering the impact of P-Delta effects (second-order analysis), which also includes stiffness reduction per the Direct Analysis Method (DM), the weight of steel in the SMF increased by approximately 5-10% compared to the designs by first-order analysis. This increased steel weight translates into increases in strength of approximately 10-15% and increases in ductility of approximately 5-10%. Elastic stiffness increases are approximately on the same order as the strength increases (10-15%).
- Based on the limited results from this study, the drift limit appears to be more influential than consideration of P-Delta effects.

Further study of seismic stability for steel special moment frames will include comprehensive collapse assessments per FEMA P695. The results from this paper will also be combined with similar assessments for other types of steel seismic lateral force-resisting systems to develop design provisions that will aim to enhance safety and economy for future design.

## 5. Acknowledgments

This study is supported by the American Institute of Steel Construction. The opinions, findings, and conclusions in this paper are those of the authors and do not necessarily reflect the views of those acknowledged here.

## 6. Disclaimer

Commercial software may have been used in the preparation of information contributing to this paper. Identification in this paper is not intended to imply recommendation or endorsement by NIST, nor is it intended to imply that such software is necessarily the best available for the purpose. NIST policy is to use the International System of Units in all its published materials. However, in this paper, some information is presented in U.S. customary units as this is the preferred system of units in the U.S. earthquake engineering industry.



 

## 7. References

[1] MacRae GA (1994): P-Δ effects on single-degree-of-freedom structures in earthquakes. *Earthquake spectra*, **10** (3), 539-568.

[2] Krawinkler H, Seneviratna GD (1998): Pros and cons of a pushover analysis of seismic performance evaluation. *Engineering structures*, **20** (4-6), 452-464.

[3] Gupta A, Krawinkler H (2000): Estimation of seismic drift demands for frame structures. *Earthquake Engineering & Structural Dynamics*, **29** (9), 1287-1305.

[4] ASCE (2017): Minimum Design Loads for Buildings and Other Structures. *ASCE/SEI 7-16,* American Society of Civil Engineers, Reston, VA.

[5] AISC (2016a): Specification for Structural Steel Buildings. *ANSI/AISC 360-16*, American Institute of Steel Construction, Chicago, IL, USA.

[6] AISC (2016b): Seismic Provisions for Structural Steel Buildings. *ANSI/AISC 341-16*, American Institute of Steel Construction, Chicago, IL, USA.

[7] Zaruma S, Fahnestock LA (2018): Assessment of design parameters influencing seismic collapse performance of buckling-restrained braced frames. *Soil Dynamics and Earthquake Engineering*, **113**, 35-46.

[8] Mathur K., Fahnestock LA, Okazaki T, Parkolap MJ (2011): Impact of residual stresses and initial imperfections on the seismic response of steel moment frames. *Journal of Structural Engineering*, **138** (7), 942-951.

[9] ASCE (2017): Seismic Evaluation and Retrofit of Existing Buildings. *ASCE/SEI 41-17*, American Society of Civil Engineers, Reston, VA.

[10] Harris III JL, Speicher MS (2018): Assessment of Performance-Based Seismic Design Methods in ASCE 41 for New Steel Buildings: Special Moment Frames. *Earthquake Spectra*, **34** (3), 977-999.

[11] Speicher MS, Harris III JL (2016a): Collapse prevention seismic performance assessment of new special concentrically braced frames using ASCE 41. *Engineering Structures*, **126**, 652-666.

[12] Speicher MS, Harris III JL (2016b): Collapse prevention seismic performance assessment of new eccentrically braced frames using ASCE 41. *Engineering Structures*, **117**, 344-357.

[13] Speicher MS, Harris III JL (2018): Collapse Prevention seismic performance assessment of new buckling-restrained braced frames using ASCE 41. *Engineering structures*, **164**, 274-289.

[14] Speicher MS, Dukes JD, Wong KW (2020): Collapse Risk of Steel Special Moment Frames per FEMA P695. *NIST Technical Note 2084*, National Institute of Standards and Technology, Gaithersburg, MD, USA. https://doi.org/10.6028/NIST.TN.2084.

[15] FEMA (2009): Quantification of building seismic performance factors. *FEMA P695*, Federal Emergency Management Agency, Washington DC, USA.

[16] Harris III JL, Speicher MS (2015): Assessment of First Generation Performance-Based Seismic Design Methods for New Steel Buildings Volume 1: Special Moment Frames. *NIST Technical Note 1863-1*, National Institute of Standards and Technology, Gaithersburg, MD, USA. http://dx.doi.org/10.6028/NIST.TN.1863-1.

[17] McKenna F, Fenves GL, Scott MH (2000): Open system for earthquake engineering simulation, version 2.5.0. *University of California, Berkeley*, CA, USA.

[18] Ibarra LF, Medina RA, Krawinkler H (2005): Hysteretic models that incorporate strength and stiffness deterioration. *Earthquake engineering & structural dynamics*, **34** (12), 1489-1511.

[19] Lignos DG, Krawinkler H (2010): Deterioration modeling of steel components in support of collapse prediction of steel moment frames under earthquake loading. *Journal of Structural Engineering*, **137** (11), 1291-1302.

[20] ATC (2017): Guidelines for Nonlinear Structural Analysis for Design of Buildings: Part IIa – Steel Moment Frames. *NIST GCR 17-917-46v2*, Applied Technology Council, Redwood City, CA, USA

[21] Krawinkler H (1978): Shear in beam-column joints in seismic design of steel frames. *Engineering Journal*, **15** (3).



 